Science Advances
AAAS

advances.sciencemag.org/cgi/content/full/4/7/eaat0415/DC1

Supplementary Materials for

Hybrid chiral domain walls and skyrmions in magnetic multilayers

William Legrand, Jean-Yves Chauleau, Davide Maccariello, Nicolas Reyren, Sophie Collin, Karim Bouzehouane, Nicolas Jaouen, Vincent Cros*, Albert Fert

*Corresponding author. Email: vincent.cros@cnrs-thales.fr

Published 20 July 2018, *Sci. Adv.* **4**, eaat0415 (2018)
DOI: 10.1126/sciadv.aat0415

This PDF file includes:

Section S1. Detailed description of the hybrid chiral spin textures found in simulations

We proceed here with a more detailed description of the results shown in Fig. 1 of the main text, in order to highlight some noticeable features of the hybrid chiral DWs. We noticed that (a) the DW width varies through the multilayer thickness ; (b) the z component of the DW magnetisation m_z cannot be simply assumed to follow an arctan function in all layers and none of the usual models allow to fit correctly the DW magnetisation structure.

Regarding point (a), we reproduce here in Fig. S1 the different representations of the DW profile from Fig. 1 in the main text, with the detailed layer by layer $\theta(x)$ profiles: as can be seen from the $\theta(x)$ profiles of Figs. 1e–h, the DW width varies significantly among the different layers. Again due to dipolar effects, the central, Bloch wall part is more compact than the Néel wall parts at top and bottom which extend over a larger width. Overall, the DW widths in the different layers vary significantly, by more than a factor of 2, as can be seen from the slopes at the center of the $\theta(x)$ profiles.

Regarding point (b), we find that in any individual layer of the stack, the DW profile cannot be properly described by the classical models. On the graphs of Figs. 1e–h, we add the average over all layers of the $\theta(x)$ profile of the micromagnetic model (orange lines), the DW profile (uniform along z) predicted by the so-called K_{eff} model (black lines), a model in which the multilayer is treated as an effective magnetic media and the DWs as non-interacting (see Methods for details), and the DW profile (also

uniform along z) predicted by the (Δ,λ,ψ) model (*15*) (green lines). It can be clearly seen that the two latter profiles fail to reproduce both the exact shape of the DW, notably in the region of the tail, as well as the DW width. Notably, this difference demonstrates that the actual DW shapes are different from the commonly used arctan profile. Moreover, as can be seen from the strongly x dependent $\psi(x)$ profiles in Figs. 1i–l, the Bloch-Néel character of the DW in each layer varies across the DW (along x), instead of being fixed. As a consequence of the DW being partially Bloch, and only in the intermediate layers (combined x and z dependence of ψ), with varying DW widths, the average transverse magnetisation of the DWs is altered and DW energies turn to be significantly different from any simple model predictions. We note that when D exceeds $2.5\,\mathrm{mJ\,m^{-2}}$, the DWs resemble pure Néel DWs, and classical models get accurate, with a good agreement between micromagnetic and classical models.

Section S2. Details of the determination of DMI with complete micromagnetic simulations

We describe in this section our method for determining the magnitude of the DMI even in the presence of hybrid chiral spin textures. We first remind how, in the usual case of homochiral DWs and assuming that the demagnetised state observed with MFM is very close to the state of minimum energy given parallel stripe domains, it is possible to determine the DW energy σ_{dw} and deduce a rough estimation of the DMI magnitude $|D|$ from the domain periodicity λ with the so-called K_{eff} model. For uncoupled, independent DWs, separating domains of size $\lambda/2$ much larger than the

DW width $\Delta = \sqrt{A/K}$, there exist two straightforward approximations for K and thus for the DW energy (*47*). For single and ultrathin layers (of thickness $t \ll \Delta$), the demagnetising fields favour in-plane magnetisation inside the DW so that the anisotropy affecting the DW is the effective perpendicular anisotropy $K = K_u - \mu_0 M_s^2/2$. On the contrary, for thick layers ($t \gg \Delta$), the in-plane alignment inside the DW is disfavoured and $K = K_u + \mu_0 M_s^2/2$. However, these approximations cannot be applied in the intermediate thickness regime, which is the relevant case for magnetic multilayers such as the ones considered here, where both Δ and t are in the order of 10 nm. Following Ref. (*47*), we can refine the formula of the DW anisotropy K by assuming that for calculating demagnetising fields roughly, the DW can be considered as a monodomain magnetic body of width 2Δ, height t and infinite length. Due to the arctan profile of the DW, an elliptic shape is a good approximation. Inserting the demagnetising factors of the elliptic cylinder (*48*)

$$\begin{aligned} N_x &= \frac{t}{t+2\Delta} \\ N_z &= \frac{2\Delta}{t+2\Delta} \end{aligned}$$

in the effective anisotropy K gives a simple expression which allows to find the DW width by solving

$$\Delta = \sqrt{\frac{A}{K_u + \frac{\mu_0 M_s^2}{2}\frac{(t-2\Delta)}{(t+2\Delta)}}}$$

By summing the contributions of exchange, DMI, anisotropy and demagnetising fields in the elliptic body (*10*), the DW energy is then

$$\sigma_{\mathrm{dw}} = 2A/\Delta + 2K_u\Delta - \pi\,|D| + \frac{\mu_0 M_s^2}{2} 2\Delta \left(\frac{t-2\Delta}{t+2\Delta}\right)$$

Concerning the demagnetising energy arising from the domains, in the zero width (as $\lambda \gg \Delta \sim 0$) model we get (*42*)

$$\epsilon_{\mathrm{demag}} = 2\mu_0 M_s^2 \frac{\lambda}{t} \frac{1}{\pi^3} \sum_{n \geqslant 1, \mathrm{odd}}^{\infty} \frac{1}{n^3} \left(1 - \mathrm{e}^{-2\pi n t/\lambda}\right)$$

which allows one to find σ_{dw} from the observed λ. Indeed, by minimising the total energy $\epsilon_{\mathrm{tot}} = 2\sigma_{\mathrm{dw}}/\lambda + \epsilon_{\mathrm{demag}}$ relative to λ we get

$$\sigma_{\mathrm{dw}} = \mu_0 M_s^2 \frac{\lambda^2}{t} \frac{1}{\pi^3} \sum_{n \geqslant 1,\ \mathrm{odd}}^{\infty} \frac{1}{n^3} \left(1 - \mathrm{e}^{-2\pi n t/\lambda} - \frac{2\pi n t}{\lambda} \mathrm{e}^{-2\pi n t/\lambda}\right)$$

which allows one to find D by equaling it to the previous expression of σ_{dw} as we know M_s, K_u, and A estimated to be $10\,\mathrm{pJ\,m^{-1}}$. A was obtained by determining the Curie temperature from temperature-dependent SQUID measurements. To apply this K_{eff} model, the multilayer is treated as an effective magnetic medium filled with diluted moments. Note that this assumption is valid as long as the periodicity of the stack is not significantly larger than the DW size (*15*), which is always verified for the samples considered here.

This characterisation method has led to the evidence of a significant DMI in magnetic multilayers with broken inversion symmetry (*7, 12*). It has however been pointed out recently that such measurements can be largely erroneous when neglecting stray-field effects on the DW size and spacing, so that a more comprehensive model is required for multilayers (*15*). When dipolar interactions become significant but the DW internal configuration remains uniform, a more detailed model such as the (Δ,λ,ψ) is more accurate (*15*). Nevertheless, we now suspect that complex DW or skyrmion structures can arise in magnetic multilayers depending of the relative

strengths of dipolar interactions and DMI, which calls for a more careful analysis of their spin textures (*16–18*).

In order to find the strength of the DMI in the stripe domains configuration without making assumptions on the DW profiles, we performed micromagnetic simulations with the Mumax3 solver (*49*) in a 3D mesh accounting for the full geometry of the multilayers. The simulation volume is $\lambda \pm d\lambda \times 32\,\mathrm{nm} \times Np$, respectively, in the x, y and z directions. Two DWs separating up, down and up domains are initialised at $(-\lambda \pm d\lambda)/4$ and $(\lambda \pm d\lambda)/4$, which corresponds to the $\lambda \pm d\lambda$ periodicity of the stripes. Periodic boundary conditions inclusive of the periodic stray fields calculated for 64×64 identical neighbors in the x and y directions were introduced. The x cell size was 0.25 nm for the XRMS multilayers series. The z cell size was 0.2 nm, or 0.1 nm when required by the values of layer spacing p and thickness t. Simulations are performed at 0 K.

Given the experimental value of λ, the simulation is initialised with its DWs having a $\psi = 45°$ in-plane tilt of internal moments for x sizes λ−2 nm,λ−1 nm,λ,λ+1 nm,λ+2 nm. Each system is relaxed in order to find the ground state energy density $\epsilon(\lambda)$, so that we get the local value of $d\epsilon/d\lambda$ at λ. Performing this operation for various values of D allows to find D_{full} such that $d\epsilon/d\lambda = 0$ by interpolation.

Section S3. MFM on the different samples

We present here in Fig. S2 the Magnetic Force Microscopy (MFM) images of the demagnetised multilayers that have been used in order to extract the mean domain periodicity.

Section S4. Domain wall fields–Analytical derivation

We want here to derive an analytical formula descriminating DWs that will exhibit hybrid chirality. For this we consider the fields acting on the top layer for the case of $D > 0$ (which is equivalent to consider fields on the bottom layer for $D < 0$). In order to find the dipolar field in the top layer of the multilayer, we have to find the solution for the potential ϕ of Laplace equation $\nabla^2\phi = \rho_V$ with ρ_V the volume charges and boundary conditions related to surface charges ρ_S. As was done in Lemesh et al. (*15*) we separate volume and surface magnetic charges contributions. We consider λ-periodic stripe domains in the x direction (uniform along y) and approximate the DW profile by the arctan profile (which we know to be an approximation). We note t the magnetic layer thickness, p the multilayer periodicity and N the total number of layers. Assuming a perfectly Néel DW in all layers, we can obtain the DW width Δ from the (Δ,λ,ψ) model.

We first solve for a single layer $\nabla^2\phi = 0$ with $\partial\phi/\partial z(x, \pm t/2^-) = \partial\phi/\partial z(x, \pm t/2^+) \pm \rho_S(x)$. As $\rho_S(x)$ corresponds to the charges of two opposite, alternate DW profiles (up to down and down to up) localised every $\lambda/2$, we can write (*15*)

$$\rho_S(x) = \sum_{k=-\infty}^{\infty} f_S(x) * \delta(x - k\lambda) + \sum_{k-\infty}^{\infty} -f_S(x) * \delta(x - k\lambda - \lambda/2)$$

where f corresponds to a single DW profile $f_S(x) = M_s m_z(x) = M_s \tanh(x/\Delta)$, that is, by combining all Dirac functions and swapping the derivatives in the convolution

product,

$$\rho_S(x) = \frac{f'_S(x)}{2} * g(x)$$

with

$$g(x) = \begin{cases} 1 & x \in [k\lambda; \lambda/2 + k\lambda[\\ -1 & x \in [\lambda/2 + k\lambda; \lambda + k\lambda[\end{cases}$$

As the magnetic charge distribution is λ periodic we can decompose it in Fourier series

$$\rho_S(x) = \sum_{k=-\infty}^{\infty} \bar{\rho_S}(k) \mathrm{e}^{-\frac{2\pi k x}{\lambda}}$$

and solve

$$\nabla^2 \bar{\phi}(k,z) = \frac{\partial^2 \bar{\phi}(k,z)}{\partial z^2} - \left(\frac{2\pi k}{\lambda}\right)^2 \bar{\phi}(k,z) = 0$$

with $\partial\bar{\phi}/\partial z(k, \pm t/2^-) = \partial\bar{\phi}/\partial z(\pm t/2^+) \pm \bar{\rho_S}$. By properties of the Fourier transform defined as

$$\bar{f}(\xi) = \frac{1}{\sqrt{2\pi}} \int f(x) \mathrm{e}^{-i\xi x} dx$$

we know that

$$\bar{\rho_S} = \overline{f'_S/2 * g} = \sqrt{2\pi} \left(\overline{f'_S} \bar{g}\right)/2 = \sqrt{2\pi} i \xi \overline{f_S} \bar{g}/2$$

so that for positive integer k

$$\begin{aligned} \bar{\rho_S}(\frac{2\pi k}{\lambda}) &= \frac{\sqrt{2\pi} i \pi k}{\lambda} \left[-iM_s\Delta\sqrt{\frac{\pi}{2}} \operatorname{csch}\left(\frac{\pi^2 \Delta k}{\lambda}\right)\right] \left[-\frac{4i}{\sqrt{2\pi}k} \sin^2\left(\frac{k\pi}{2}\right)\right] \\ &= -i\sqrt{\frac{\pi}{2}} \frac{4\pi M_s \Delta}{\lambda} \sin^2\left(\frac{k\pi}{2}\right) \operatorname{csch}\left(\frac{\pi^2 \Delta k}{\lambda}\right) \end{aligned}$$

Using the boundary conditions to solve Laplace equation (*45*) above the layer we find for $z > t/2$

$$\phi(x,z) = \sum_{k=1}^{\infty} \frac{2M_s\Delta}{k} \sin^2\left(\frac{\pi k}{2}\right) \operatorname{csch}\left(\frac{\pi^2 \Delta k}{\lambda}\right) \sinh\left(\frac{\pi k t}{\lambda}\right) \sin\left(\frac{2\pi k x}{\lambda}\right) \mathrm{e}^{-\frac{2\pi k z}{\lambda}}$$

with $x = 0$ in the center of the DW between down and up domains. For a multilayer there are N layers located at $p/2 + kp$ with $0 \leq k \leq N-1$. In the top layer, the interlayer interaction field will then be the sum of all other layers stray fields

$$B_{\mathrm{dip,S}}(x) = -\mu_0 \frac{\partial}{\partial x}\left[\sum_{n=1}^{N-1} \phi(x, np)\right]$$

that is by grouping the exponent sum

$$\begin{aligned} B_{\mathrm{dip,S}}(x) &= -\mu_0 \frac{\partial}{\partial x}\left[\sum_{k=1,\mathrm{odd}}^{\infty} \frac{2M_s\Delta}{k} \operatorname{csch}\left(\frac{\pi^2\Delta k}{\lambda}\right) \sinh\left(\frac{\pi k t}{\lambda}\right) \sin\left(\frac{2\pi k x}{\lambda}\right) \frac{\mathrm{e}^{-\frac{2\pi k p}{\lambda}} - \mathrm{e}^{-\frac{2\pi k N p}{\lambda}}}{1 - \mathrm{e}^{-\frac{2\pi k p}{\lambda}}}\right] \\ &= -\mu_0 \sum_{k=1,\mathrm{odd}}^{\infty} \frac{4\pi M_s\Delta}{\lambda} \operatorname{csch}\left(\frac{\pi^2\Delta k}{\lambda}\right) \sinh\left(\frac{\pi k t}{\lambda}\right) \cos\left(\frac{2\pi k x}{\lambda}\right) \frac{\mathrm{e}^{-\frac{2\pi k p}{\lambda}} - \mathrm{e}^{-\frac{2\pi k N p}{\lambda}}}{1 - \mathrm{e}^{-\frac{2\pi k p}{\lambda}}} \end{aligned}$$

which can be determined numerically.

We can now solve for a single layer $\nabla^2\phi = \rho_V(x)$ for $|z| < t/2$ and $\nabla^2\phi = 0$ for $|z| > t/2$, with continuity of $\partial\phi/\partial z$ at $z = \pm t/2$. We have again

$$\rho_V(x) = \sum_{k=-\infty}^{\infty} f_V(x) * \delta(x - k\lambda) + \sum_{k-\infty}^{\infty} -f_V(x) * \delta(x - k\lambda - \lambda/2)$$

with

$$f_V(x) = -M_s \nabla \cdot \mathbf{m} = -M_s \frac{\partial m_x}{\partial x} = \frac{M_s}{\Delta} \frac{\tanh(x/\Delta)}{\cosh(x/\Delta)}$$

the volume charges for a single DW. Similar to ρ_S we get $\rho_V(x) = [f_V'(x) * g(x)]/2$ and for positive integer k,

$$\begin{aligned} \bar{\rho_V}(\frac{2\pi k}{\lambda}) &= \overline{f_V'/2 * g}(k) = \sqrt{2\pi} i\,(2\pi k/\lambda)\,\overline{f_V}\bar{g}/2 \\ &= \frac{\sqrt{2\pi} i \pi k}{\lambda}\left[iM_s\Delta \frac{2\pi k}{\lambda}\sqrt{\frac{\pi}{2}} \operatorname{sech}\left(\frac{\pi^2\Delta k}{\lambda}\right)\right]\left[-\frac{4i}{\sqrt{2\pi k}} \sin^2\left(\frac{k\pi}{2}\right)\right] \\ &= -i\sqrt{\frac{\pi}{2}} \frac{-8\pi^2 M_s\Delta k}{\lambda^2} \operatorname{sech}\left(\frac{\pi^2\Delta k}{\lambda}\right) \sin^2\left(\frac{k\pi}{2}\right) \end{aligned}$$

Using the boundary continuity to solve Laplace equation above the layer we find for $z > t/2$

$$\phi(x,z) = \sum_{k=1}^{\infty} \frac{2M_s\Delta}{k} \sin^2\left(\frac{\pi k}{2}\right) \operatorname{sech}\left(\frac{\pi^2\Delta k}{\lambda}\right) \sinh\left(\frac{\pi k t}{\lambda}\right) \sin\left(\frac{2\pi k x}{\lambda}\right) \mathrm{e}^{-\frac{2\pi k z}{\lambda}}$$

so that

$$B_{\mathrm{dip,V}}(x) = -\mu_0 \sum_{k=1,\mathrm{odd}}^{\infty} \frac{4\pi M_s\Delta}{\lambda} \operatorname{sech}\left(\frac{\pi^2\Delta k}{\lambda}\right) \sinh\left(\frac{\pi k t}{\lambda}\right) \cos\left(\frac{2\pi k x}{\lambda}\right) \frac{\mathrm{e}^{-\frac{2\pi k p}{\lambda}} - \mathrm{e}^{-\frac{2\pi k N p}{\lambda}}}{1 - \mathrm{e}^{-\frac{2\pi k p}{\lambda}}}$$

One still has to consider the self-demagnetising field of the top layer itself. The surface charges distribution does not contribute to the z-average of the field as it generates a field antisymmetric in z. However the volume charges contribution must be considered. Solving again the Laplace equation but inside the magnetic layer ($|z| < t/2$) we find

$$B_{\mathrm{dip}}(x,z) = \mu_0 \sum_{k=1,\mathrm{odd}}^{\infty} \frac{4\pi M_s\Delta}{\lambda} \operatorname{sech}\left(\frac{\pi^2\Delta k}{\lambda}\right) \cos\left(\frac{2\pi k x}{\lambda}\right) \left[\cosh\left(\frac{2\pi k z}{\lambda}\right) \mathrm{e}^{\frac{\pi k t}{\lambda}} - 1\right]$$

that we can average between $z = -t/2$ and $z = t/2$ to obtain the horizontal component of the self-interaction field of the top layer

$$B_{\mathrm{dip,self}}(x) = \mu_0 \sum_{k=1,\mathrm{odd}}^{\infty} \frac{4\pi M_s\Delta}{\lambda} \operatorname{sech}\left(\frac{\pi^2\Delta k}{\lambda}\right) \cos\left(\frac{2\pi k x}{\lambda}\right) \left[\frac{1 - \mathrm{e}^{-\frac{2\pi k t}{\lambda}}}{2} \frac{\lambda}{\pi k t} - 1\right]$$

The dipolar interlayer interaction pushing to reverse the DW is then

$$B_{\mathrm{dip}}(x) = B_{\mathrm{dip,S}}(x) + B_{\mathrm{dip,V}}(x)$$

while the total dipolar field is finally

$$B_{\mathrm{dip,t}}(x) = B_{\mathrm{dip,S}}(x) + B_{\mathrm{dip,V}}(x) + B_{\mathrm{dip,self}}(x)$$

The DMI internal field along x of the Néel DW can be described by (*10*)

$$B_{\mathrm{dmi}}(x) = \frac{2D}{M_s}\frac{\partial m_z}{\partial x} = \frac{2D}{M_s\Delta}\,\mathrm{sech}^2\left(\frac{x}{\Delta}\right)$$

as we approximate it to a classical tan profile.

In order to compare the strengths of B_{dip} and B_{dmi}, we evaluate their actions locally by integration across the DW

$$\mathcal{A} = \frac{1}{6\Delta}\int_{-3\Delta}^{3\Delta} B(x)m_x(x)dx$$

that corresponds to the in-plane rotation driving force acting on the DW of the top layer.

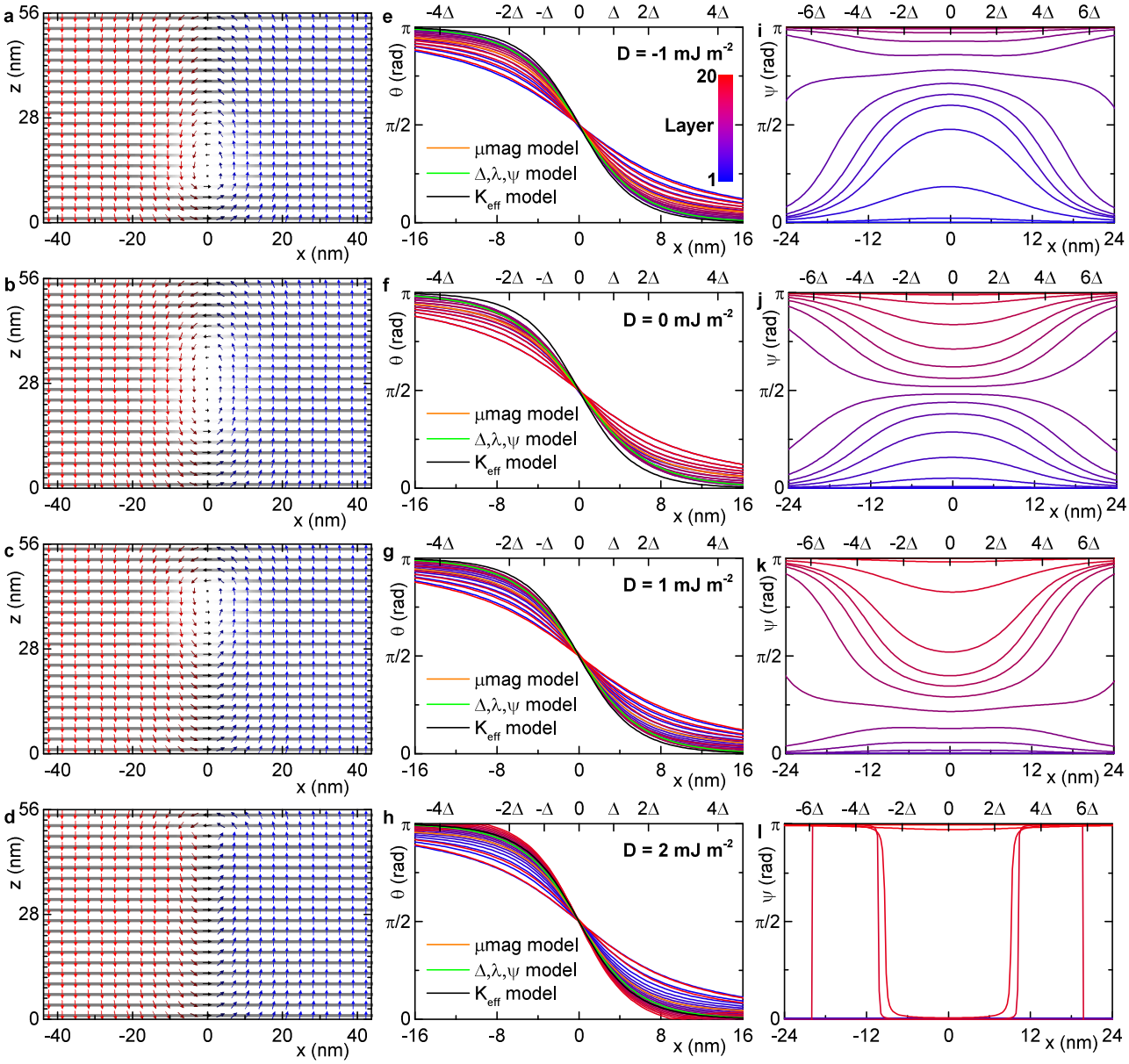

Fig. S1. Detailed version of Fig. 1. a–d. Cross-sectional view of a half simulation volume for $[X(1)/Co(0.8)/Z(1)]_{20}$ multilayer with D = -1.0, 0.0, 1.0 and 2.0 mJ m^{-2}, respectively. Arrows point in the direction of the magnetisation, m_z is given by the colour of the arrows from red (-1) to blue (+1), while m_y is displayed by the colour of the grid from black (-1) to white (+1). e–h. Polar angle θ inside the DW in each layer for D = -1.0–2.0 mJ m^{-2}. The blue to red lines correspond to layers from bottom to top (see colour scale in e.), while the orange line is the average θ across the thickness. Green and black lines are the profiles as given by the (Δ,λ,ψ) and K_{eff} models, respectively. i–l. Azimuthal angle ψ inside the DW in each layer for D = -1.0–2.0 mJ m^{-2}. The blue to red lines again correspond to layers from bottom to top.

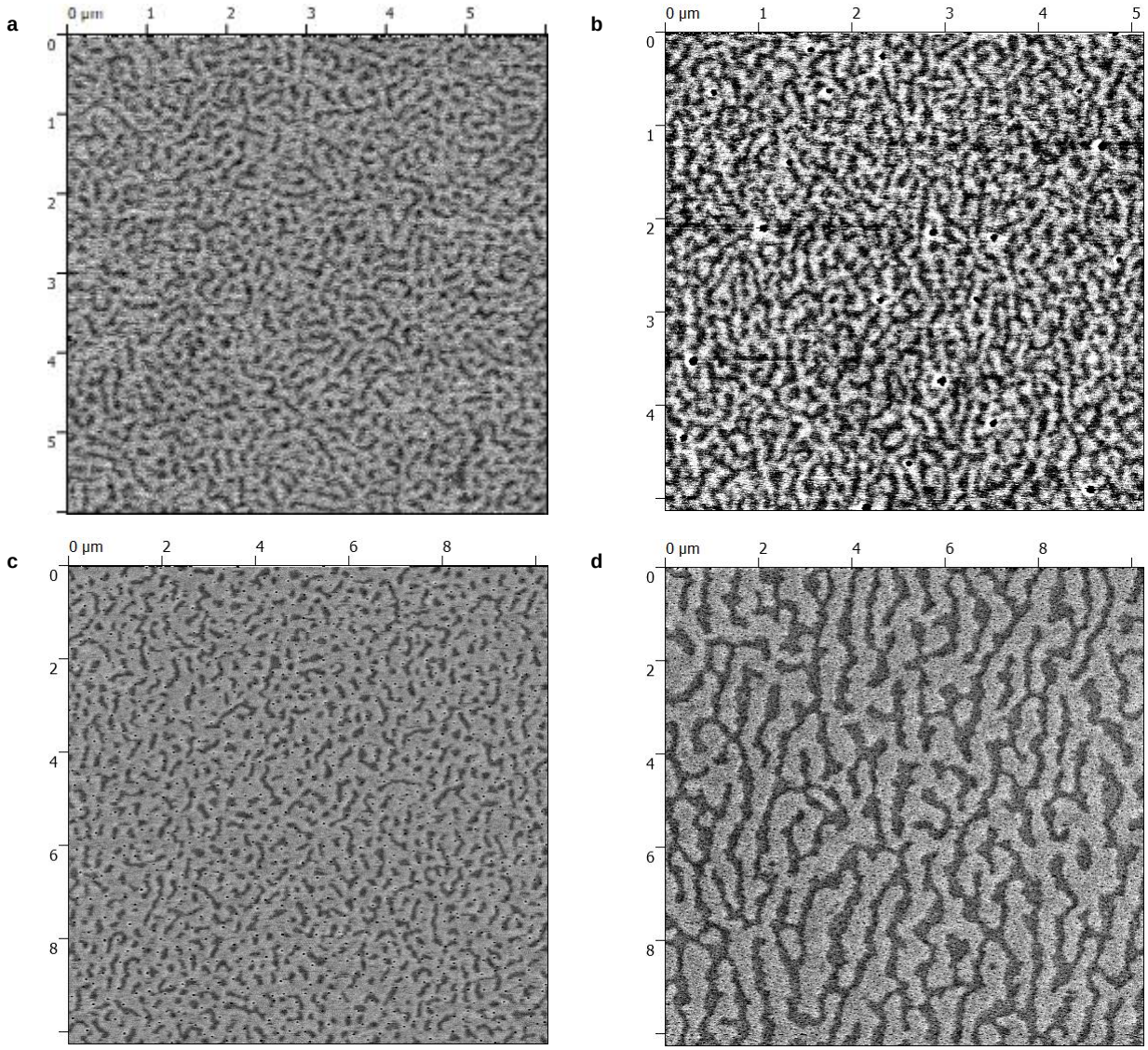
a
0 µm 1 2 3 4 5
0 1 2 3 4 5
b
0 µm 1 2 3 4 5
0 1 2 3 4
c
0 µm 2 4 6 8
0 2 4 6 8
d
0 µm 2 4 6 8
0 2 4 6 8

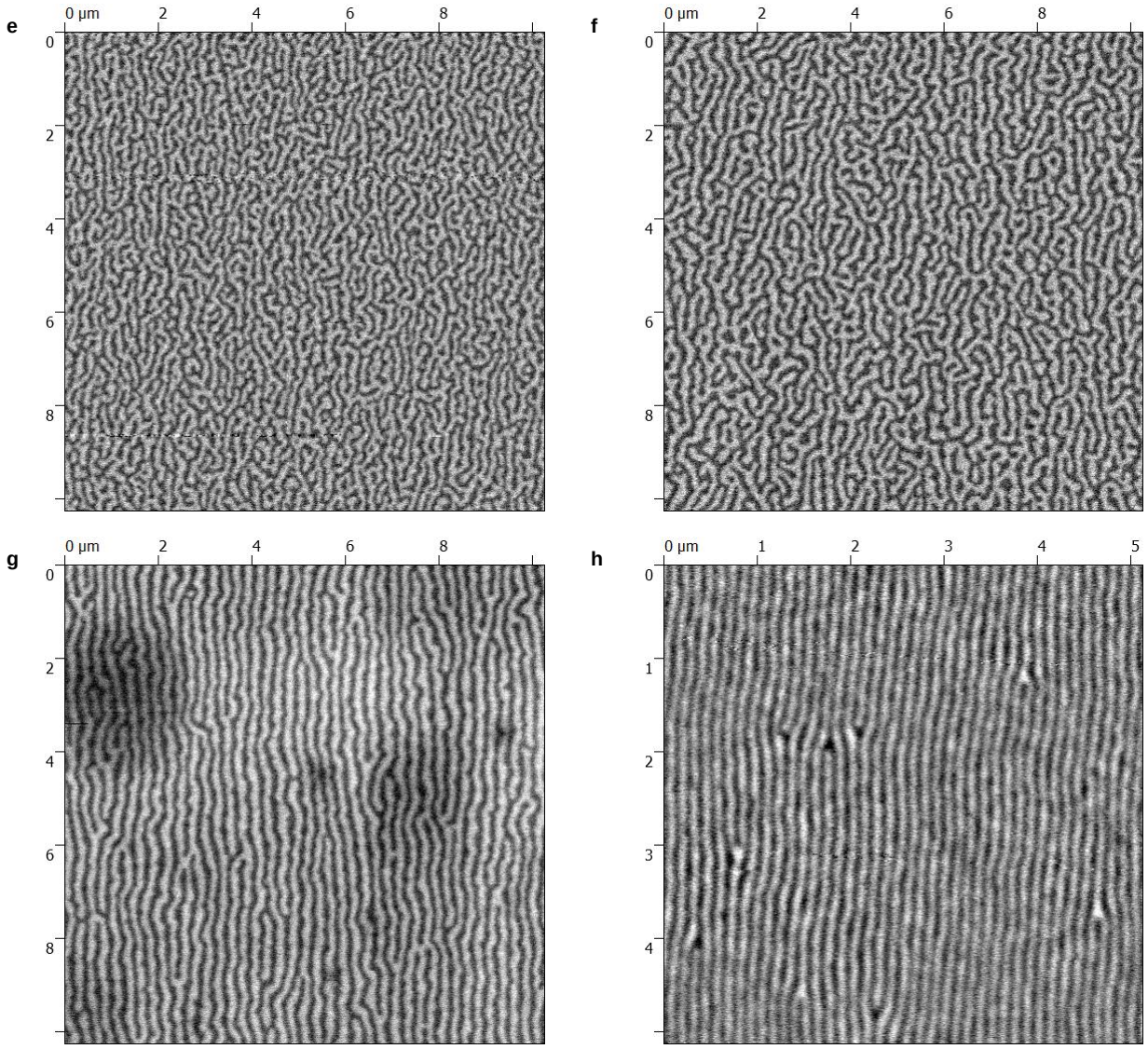
e
0 µm
2
4
6
8
0
2
4
6
8
f
0 µm
2
4
6
8
0
2
4
6
8
g
0 µm
2
4
6
8
0
2
4
6
8
h
0 µm
1
2
3
4
5
0
1
2
3
4

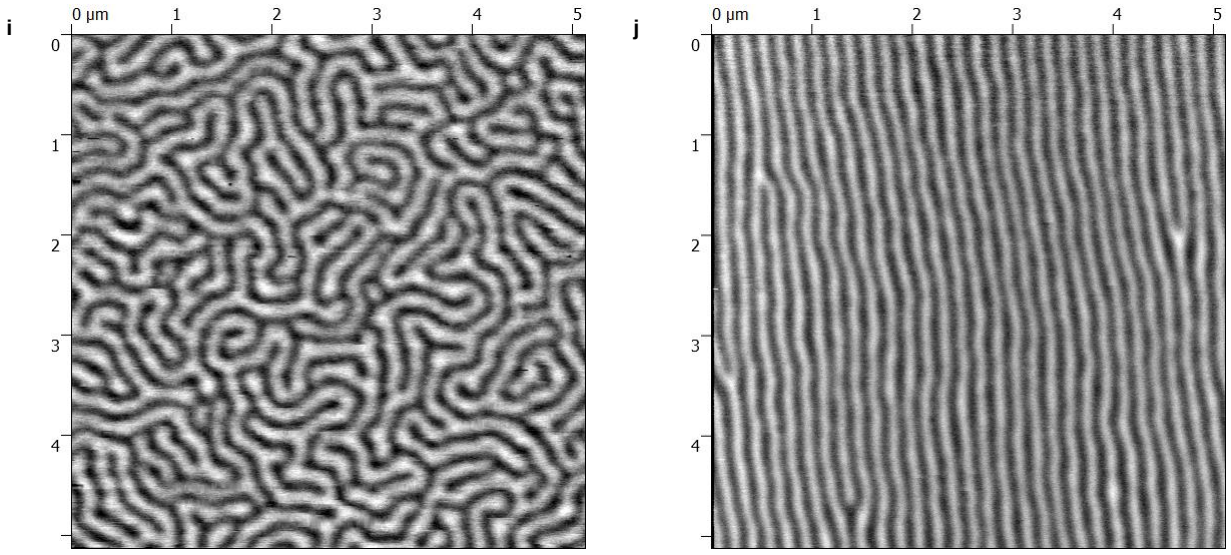

Fig. S2. MFM images of domain structures in studied multilayers. a–g. In-plane field demagnetised multilayers (I) to (VII). h. In-plane demagnetised multilayer (IX). i. Out-of-plane and j. in-plane demagnetised multilayer (VIII).